Thermoresponsive low-power light upconverting polymer nanoparticles

David C. Thévenaz,[a] Angelo Monguzzi,[b] Dimitri Vanhecke,[a] Roberto Vadrucci,[a] Francesco Meinardi,[b] Yoan C. Simon*[ac] and Christoph Weder*[a]

Conceptual insights

Sensitized triplet-triplet annihilation light upconversion permits converting low-intensity radiation into light of higher frequency. Known in solution for half a century, this process was only recently achieved in solid polymers and nanoobjects. For biomedical imaging applications, nanoparticles which offer efficient upconversion in aerated aqueous environments are needed. We show that polymer nanoparticles in which the proximity of covalently attached chromophores supports efficient energy transfers and exciton diffusion meet this requirement. The polymer not only plays a structural and protective role. We show that its physical state, which can be reversibly switched, significantly impacts the nanoparticles' photophysical properties.

www.rsc.org/

We report highly efficient sensitized triplet-triplet annihilation based upconversion in aqueus suspensions of nanoparticles prepared from a 9,10-diphenylanthracene-terminated poly(ε-caprolactone) and platinum octaethylporphyrin as sensitizer. The particles' upconversion characteristics are strongly temperature-dependent. This feature permits insights into the mechanisms enabling the process in the nanoparticle environment, and the specific temperature range in which the photophysical parameters change is suitable for live cell and in vivo temperature sensing.

Sensitized triplet-triplet annihilation light upconversion (*s*TTA-UC) is a photophysical process that has been known to occur in solutions of suitable chromophore pairs for fifty years.[1,2] After attracting renewed interest in the last decade,[3-6] sTTA-UC was eventually also realized in polymers and nano-objects.[7-15] The latter are thought to be useful for applications such as bio-imaging, photo-triggered drug release, oxygen sensing, and photo-chemical reactions.[11,14,15] The *s*TTA-UC process is based on the interplay between two chromophores, a sensitizer that absorbs light and after intersystem crossing transfers the exciton to an emitter *via* triplet-triplet (Dexter) energy transfer. The formation of an encounter complex between two emitter triplets and their annihilation (TTA) eventually results in the population of an emitter singlet excited state, from which high-energy fluorescence occurs.[14] The Dexter energy transfer and the TTA require molecular orbital overlap between the involved species.[16] Efficient *s*TTA-UC is thus observed in dilute solutions in which the chromophore molecules display high translational mobility[14,16] or materials with densely packed chromophores, where exciton migration is feasible.[7,17-24]

TTA upconverting nanoconstructs are useful as bio-probes, as some of the drawbacks associated with downconverting fluorescent nanoparticles (e.g. scattering of the excitation light with a short wavelength, tissue autofluorescence) can be alleviated.[8,10-12,25-27] The prospect of using near infrared (IR) to visible upconverting chromophores is particularly attractive, as excitation in the near IR allows for better tissue penetration and reduced photodamage.[28] Several strategies have been proposed to fabricate nanoobjects that display *s*TTA-UC. The incorporation of sTTA-UC chromophore pairs into nanocapsules with a liquid core was reported by several groups.[10,12,25] This general design takes advantage of the high mobility of the chromophore molecules in a liquid environment, which is one way to achieve high sTTA-UC efficiency. In other studies, sTTA-UC chromophores were stabilized by hydrophobic interactions in the core of micellar structures.[26,29] Growing a silica shell around these micelles afforded nanoparticles that could be used for in vivo imaging.[26,27] An alternative design approach relies on doping the hydrophobic core of cross-linked polymer nanoparticles with sensitizer and emitter molecules.[7,8] Recently, high concentrations of sTTA-UC chromophores were introduced into polymers by covalent attachment.[13,17,18] This strategy prevents phase separation and enables exciton migration, and remained largely unexploited for the design of nanoobjects. We here report sTTA-UC polymer nanoparticles that utilize this approach and display an unprecedented quantum yield of ~ 7.5% as well as strongly temperature-dependent sTTA-UC

[a] *Adolphe Merkle Institute, University of Fribourg, Chemin des Verdiers 4, 1700, Fribourg, Switzerland, E-mail: christoph.weder@unifr.ch*

[b] *Dipartimento di Scienza dei Materiali, Università of Milano-Bicocca, via Cozzi 55, I-20125 Milano, Italy*

[c] *School of Polymers and High Performance Materials, University of Southern Mississippi, 118 College Dr., Hattiesburg, MS 39406, USA, E-mail: Yoan.Simon@usm.edu*

characteristics. The nanoparticles were prepared by a microemulsion technique in the presence of a surfactant and consist of a low-molecular weight poly(ε-caprolactone) that was end-functionalized with the well-known emitter 9,10-diphenylanthracene (DPA-PCL-OH, **3**) and of the matching sensitizer platinum octaethylporphyrin (PtOEP, Fig. 1a,b). PCL was selected due to its biocompatible and biodegradable nature, and we discovered that its semi-crystalline character causes the sTTA-UC mechanism to be strongly temperature-dependent,[30] with an increase of the emitter triplet state quenching rate and a sharp drop of the sTTA-UC efficiency around physiological temperature (*ca.* 40 °C). This thermoresponsive behavior offers mechanistic insights and appears useful for in vivo temperature sensing.

The synthesis of DPA-PCL-OH (**3**) is outlined in Fig. 1a. A hydroxyl-functionalized DPA (**2**)[19] was used to initiate the ring-opening polymerization of ε-caprolactone with $Sn(oct)_2$ as catalyst. Via the ratio of DPA to ε-caprolactone, the degree of polymerization was kept low and the DPA content high. The number-average molecular weight, M_n ~ 1,750 g mol^{-1} (ESI Table S1) of **3** and the covalent attachment of DPA were determined/confirmed by NMR spectroscopy, size-exclusion chromatography (SEC), and MALDI-TOF mass spectrometry (ESI Figs. S1-S4). A clear shift was observed for the benzylic proton in the ^{1}H NMR spectrum of compound **3** (5.31 ppm, ESI Fig. S1) vis-à-vis **2** (4.91 ppm)[19] and the absence of free DPA was confirmed by SEC data acquired using UV detection (ESI Fig. S4). Finally, the expected mass pattern for **3** was confirmed by MALDI-TOF spectroscopy (ESI Fig. S3). Thermogravimetric analysis reveals that **3** is stable up to above 200 °C (ESI Fig. S6) and its differential scanning calorimetry (DSC) trace shows that the material melts in the range of ~ 40-45 °C (ESI Fig. S5), i.e., in a similar range as DPA-free PCL of similar M_n (ESI Fig. S7). The melting transition is reflected by two endothermic transitions at 40 and 45°C, which is typical for low-molecular weight PCL.[31]

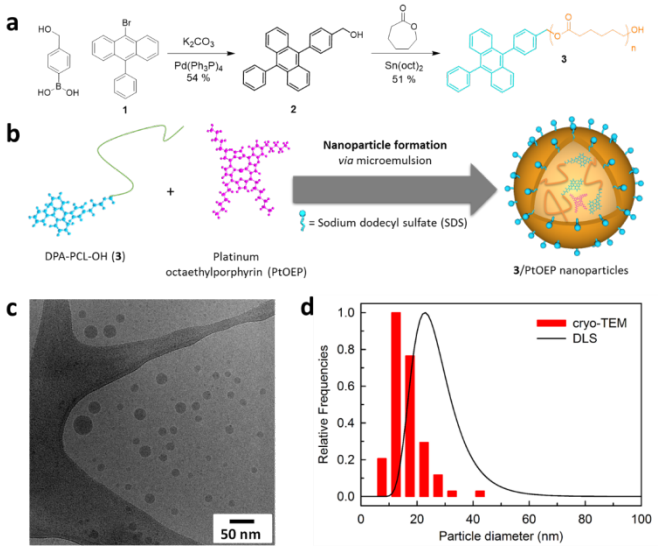

Fig. 1. (a) Synthesis of the 9,10-diphenylanthracene-terminated poly(ε-caprolactone) (**3**). (b) Schematic representation of the nanoparticle formation process and of the components used. (c) Representative cryo-TEM image of an aqueous suspension of **3**/PtOEP nanoparticles (~ 5 mg/mL). (d) Size distributions of **3**/PtOEP nanoparticles obtained by DLS measurements of an aqueous suspension (~ 0.5 mg/mL) at a scattering angle of 90° (black line) and by analysis of cryo-TEM images (red bars).

A microemulsion method was adapted to prepare the up-converting nanoparticles.[13] DPA-PCL-OH (**3**) and PtOEP were dissolved in dichloromethane (DCM) and the organic phase was combined with a solution of the surfactant sodium dodecyl sulfate (SDS) in water. The mixture was emulsified by sonication and DCM was removed under reduced pressure at room temperature to avoid thermally induced morphological changes. The morphology and dimensions of the **3**/PtOEP nanoparticles thus prepared were probed by cryo-transmission electron microscopy (cryo-TEM) and dynamic light scattering (DLS) (Fig. 1c). The cryo-TEM images reveal that the nanoparticles are spherical and polydisperse, with an average diameter of *ca.* 15 nm (Fig. 1d). The conversion of DLS data into a number-weighted distribution using a solid-sphere model results a size distribution that is slightly shifted towards larger particles, with an average diameter of *ca.* 26 nm, Fig. 1d. This discrepancy points to solvation effects in the dispersion studied by DLS or a biased distribution originating from variations of the sample visualized by cryo-TEM.[32] Control PCL/PtOEP and PCL nanoparticles (made with DPA-free PCL of similar M_n and in the latter case without sensitizer) were prepared in the same manner to explore the influence of the chromophores on the nanoparticle synthesis and to study the phosphorescence of the sensitizer within the nanoparticle matrix. Particles with similar size distributions were obtained (ESI Fig. S8), suggesting that the chromophores do not significantly impact the assembly process. Noting that certain sTTA-UC chromophores can be assembled into micellar structures in aqueous media using only a surfactant,[29] we investigated if upconverting particles would form when the microemulsion method was applied to the DPA derivative **2** and PtOEP. However, no stable suspension was obtained, suggesting that here the presence of the polymer is essential for the assembly. Aqueous suspensions of **3**/PtOEP nanoparticles display low turbidity under ambient illumination (inset Fig. 2a) and their absorption spectrum shows the characteristic bands of DPA (320-420 nm) and PtOEP (480-550 nm). By contrast, the spectrum of the PCL/PtOEP reference nanoparticles shows, as anticipated, only the absorption bands associated with the sensitizer, as reported in ESI Fig. S9.

The emission characteristics of aqueous suspensions of **3**/PtOEP and PCL/PtOEP reference particles were probed by steady-state photoluminescence spectroscopy upon excitation with a continuous wave green laser at 532 nm. The emission spectrum of the **3**/PtOEP suspension is dominated by a band at 435 nm that is characteristic of delayed DPA fluorescence and shows only weak residual PtOEP phosphorescence around 650 nm (Fig. 2a). The latter was much stronger in the case of the PCL/PtOEP reference particles, whose spectrum, like DPA in the absence of the sensitizer (ESI Fig. S10) did not show upconverted emission. The yield of the triplet-triplet energy transfer between sensitizer and the emitter molecules, $\Phi_{TT\text{-}ET}$, can be determined by comparing the integrated sensitizer phosphorescence in presence ($I_{S/E}$) and absence (I_S) of the emitter (Eq. 1). Our analysis reveals a $\Phi_{TT\text{-}ET}$ of 0.98 for the **3**/PtOEP nanoparticles, reflecting a highly efficient transfer.

$$\Phi_{TT-ET} = 1 - \frac{I_{S/E}}{I_S} \qquad (1)$$

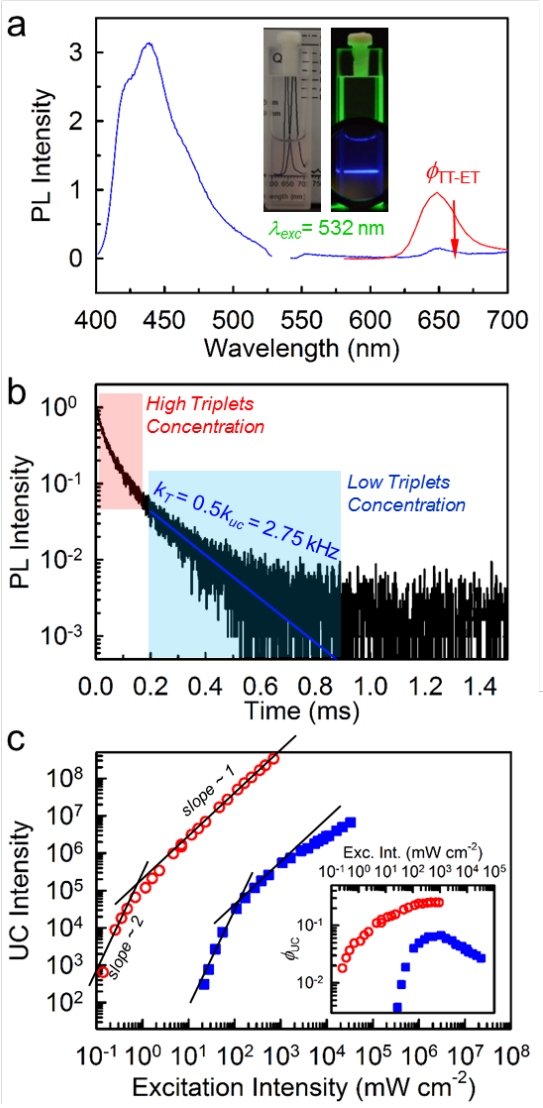

Fig. 2. (a) Photoluminescence spectra of aqueous dispersions of **3**/PtOEP and PCL/PtOEP nanoparticles upon continuous wave laser (CWL) excitation at 532 nm. The inset picture documents the low turbidity of a **3**/PtOEP nanoparticle suspension under ambient illumination (left) and the upconverted blue emission upon 532 nm excitation (right), viewed through a 500 nm short-pass filter. (b) UC luminescence decay of an aqueous **3**/PtOEP nanoparticle suspension measured at 435 nm under pulsed excitation at 532 nm. (c) Upconverted emission intensity as a function of excitation intensity of a deoxygenated standard DPA:PtOEP solution in THF ([DPA] = 10 mM, [PtOEP] = 100 μM) (red circles) and an aqueous **3**/PtOEP nanoparticle suspension (blue squares), both under CWL excitation at 532 nm. The inset shows the sTTA-UC quantum yield obtained by comparison of the data and the aforementioned DPA:PtOEP reference solution as a function of excitation intensity. All experiments were carried out with aqueous suspensions of the **3**/PtOEP nanoparticles under ambient conditions (not deoxygenated) (c ~ 5 mg/mL).

As usual for sTTA-UC, the upconverted emission decay time at 435 nm is in the range of milliseconds and it is multi–exponential.[33] The spontaneous emitter triplet decay rate k_T = 2.75 kHz can be obtained from the long-time tail of the upconverted light decay trace, when the concentration of excited triplets is low (Fig. 2b) and, therefore, TTA is a negligible recombination channel. In this regime, sTTA-UC is in any case a bimolecular process, and k_T is thus half of the experimentally measured UC decay rate k_{UC} = 5.50 kHz.[34] The excitation power threshold (I_{th}), i.e., the excitation power density at which sTTA-UC starts to work efficiently, can be determined by plotting the upconverted emission intensity as function of the excitation power density in a log-log scale, in order to evidence the transition from the quadratic to the linear regime where the annihilation yield Φ_{TTA} = 1 and the upconversion efficiency is maximum.[16] Fig. 2c shows this data for the **3**/PtOEP nanoparticle suspension and a DPA:PtOEP solution in degassed tetrahydrofuran (THF) used as a standard. The **3**/PtOEP nanoparticle suspension displays an I_{th} of 189 mW cm^{-2}, indicating that the sTTA-UC dynamics are less efficient than in the standard, where the observed threshold intensity is lower. This can be a consequence of: i) a k_T that is higher than the one commonly observed in organic solvents (<1 kHz), which makes the spontaneous recombination a more competitive mechanism; ii) the low mobility of the chromophores within the nanoparticles, which in principle limits the exciton diffusion. The sublinear dependency observed at high power densities may be due to the saturation of the excited emitter population[16] or photodamaging effects that reduce the sTTA-UC yield.

The overall upconversion yield Φ_{UC} of the **3**/PtOEP nanoparticles was determined via the comparison of the sTTA-UC emission with that of the standard solution ($\Phi_{UC,\ stand}$ = 26%). The inset of Fig. 2c shows that for both systems Φ_{UC} increases linearly with the excitation power density up to I_{th}. Above this irradiance, the nanoparticle Φ_{UC} saturates at a maximum quantum yield of 7.0 ± 1.0% and, as mentioned above, it shows a pronounced decrease as the excitation intensity is further increased. Absolute quantum yield measurements performed using an integrating sphere afforded the same result; in this case, Φ_{UC} = 7.5 ± 1.1 %. To the best of our knowledge, this value is the highest Φ_{UC} measured so far for sTTA-UC nanoparticles in water and represents a twofold improvement over the previously reported best quantum yield of 3.7% for cross-linked polystyrene nanoparticles doped with the same chromophores.[7] In order to explain the high Φ_{UC} value, it is useful to consider all the parameters affecting the UC yield Φ_{UC}:

$$\Phi_{UC} = \frac{1}{2}\Phi_{ISC}\Phi_{TT-ET} f \Phi_{TTA}\Phi_E. \qquad (2)$$

The factor ½ accounts for the fact that two incident photons are combined into one of higher energy, Φ_{ISC} is the intersystem crossing efficiency of the sensitizer, f is a statistical factor parameter describing the probability that the annihilation of two emitter triplets results in the formation of a singlet, and Φ_E is the emitter quantum efficiency. For DPA, f is 0.52 and, for PtOEP, Φ_{ISC} = 1.[16] Since above the threshold Φ_{TTA} reaches unity at high power densities and Φ_{TTET} = 0.98 (vide supra), the observed low conversion yield can be ascribed to a reduced Φ_E of DPA with respect to the high value commonly observed in a degassed dilute solution. Indeed, time-resolved PL measurements show that DPA in **3**/PtOEP is strongly quenched, resulting in a Φ_E = 30% (ESI Fig. S11). Using this value and Eq. 2, the expected maximum quantum yield $\Phi_{UC,\ th}$ for **3**/PtOEP system can be calculated to be 8.1%, which is in good agreement with the experimental findings.

Like the neat PCL, compound **3** is semicrystalline, with a melting temperature T_m ~ 40 °C in the bulk form (ESI Fig. S5). This thermal transition appears to be the origin of the evident temperature dependence of the upconversion efficiency of the present nanoparticles shown in Fig. 3a. When the temperature of the aqueous **3**/PtOEP nanoparticle suspension was increased from 20 to 60 °C, the UC emission intensity dropped rapidly and eventually became negligible. Interestingly, the effect is fully reversible as the upconverted emission intensity is fully restored upon cooling the sample (Fig. 3a). This finding appears to contradict the general paradigm of mobility-enhanced upconversion at high temperatures and points towards alternative non-radiative relaxation pathways above the melting temperature.

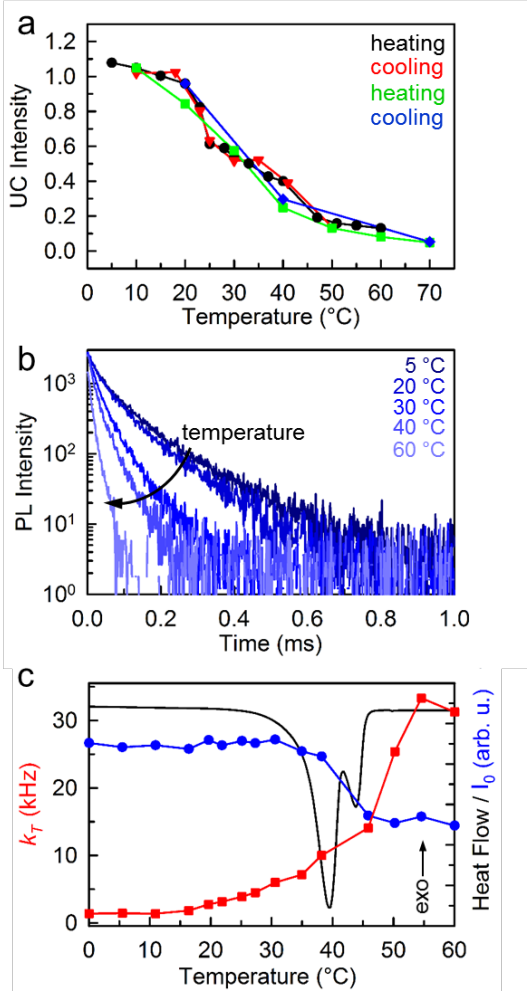

Fig. 3. (a) Temperature dependence of the integrated upconversion emission intensity of the **3**/PtOEP nanoparticles under CWL excitation at 532 nm. (b) UC luminescence decay traces, (c) UC photoluminescence intensity at time zero (I_0, blue circles), triplet decay rate (k_T, red squares), and heat flow (black line) of the **3**/PtOEP nanoparticles as a function of the temperature, monitored at 435 nm with modulated excitation at 532 nm. All experiments were carried out with aqueous suspensions of the **3**/PtOEP nanoparticles under ambient conditions (not deoxygenated) (c ~ 5 mg/mL).

The possibility that heating may impact the structural integrity of the nanoparticles was excluded by DLS, which revealed no changes of the intensity-weighted average particle diameter and polydispersity upon heating the suspension (ESI Fig. S12). In contrast, the upconversion decay dynamics vary considerably with the temperature (Fig. 3b). Two effects can be discerned: a decrease of the time-zero intensity I_0, and an increase of k_T (Fig. 3c). The data indicate that the main origin of the upconversion yield reduction observed upon heating is the enhanced spontaneous triplet decay, which increased by more than one order of magnitude upon heating. This is an unusual effect, which is not observed in sTTA-UC solutions. It is probably related to the peculiar functionalization of the DPA moiety with poly(ε-caprolactone), which makes the triplet states especially sensitive to the vibrational quenching as suggested by the measured high k_T. In addition, an overlay plot of I_0 and the DSC thermogram of polymer **3** in the bulk (Fig. 3c) shows that the time-zero intensity drop of 50% is correlated with the melt transition of the nanoparticles. This result could reflect that the average intermolecular distance between the chromophore molecules increased upon melting, while below T_m the DPA molecules were concentrated in the amorphous portion of the semicrystalline PCL matrix. Therefore, the combined effect of an increased intermolecular distance, which reduces the TTA probability, with an enhanced k_T, which increases I_{th}, results in a decrease of the number of generated fluorescent singlets at a fixed excitation intensity, which sets I_0. These findings suggest that the gain in the molecular diffusivity at high temperatures, usually associated with the softening of a polymer matrix, is not large enough to compensate for the enhanced spontaneous recombination of triplets that limits the Φ_{TTA}. Indeed, the emitter molecules have a statistical intermolecular distance that is suitable for exciton diffusion *via* a hopping mechanism regardless of the temperature. The intermolecular distance between neighboring DPA molecules, calculated assuming a stochastic distribution of 3618 chromophore molecules in a sphere with a radius of 13 nm, is ~ 1.1 nm (ESI Fig. S13). Below T_m this value is even smaller, as the DPA molecules are concentrated in the amorphous phase of the PCL. Thus, the distance between the chromophores is such that the exchange interactions are effective and matches the triplet-triplet interaction distance for DPA (a_0 = 0.91 nm) well.[35] The I_{th} data allow us to estimate the DPA triplet diffusion length, L_T, by combining Eqs. 3-5:

$$I_{th} = \frac{k_T^2}{\gamma_{TT}\alpha(E)\phi_{TTET}}, \quad (3)$$

$$\gamma_{TT} = 8\pi D a_0, \quad (4)$$

$$L_T = \sqrt{6\frac{D}{k_T}}. \quad (5)$$

Using the absorption coefficient $\alpha(E)$ = 0.64 cm^{-1} at 532 nm (ESI Fig. S9) and Eq. 3, the second-order annihilation rate constant γ_{TT} at room temperature was determined to be 2.3·10^{-11} cm^3 s^{-1}. Using this value, the exciton diffusion coefficient D was calculated to be 10^{-5} cm^2 s^{-1} and L_T = 1.4 µm. This value is much higher than the nanoparticle diameter, which confirms that under ambient conditions the exciton mobility does not limit Φ_{UC} in **3**/PtOEP. However, the quadratic dependence of I_{th} on k_T leads to a higher threshold in the nanoparticles than in the standard solution, and it further decreases

the upconversion efficiency during heating due to the enhanced spontaneous recombination that shifts I_{th} to even higher values.

Notably, the temperature dependence of the UC behavior of the **3**/PtOEP nanoparticles is significant and can be monitored by measurements of the upconverted emission intensity and the decay dynamics. The specific temperature range in which the present nanoparticles change their upconversion properties, their peculiar anti-Stokes emission and the high upconversion efficiency under aerated conditions make the material potentially useful as versatile nanothermometer for biological systems. The time-gated imaging using these UC nanoparticles would require inexpensive and easily accessible detection setups with a time resolution in the millisecond range. Therefore, the combination of anti-Stokes optical imaging with time-resolved analysis will lead to a precise high-resolution *in situ* thermal mapping of the environment.[36-38]

Conclusions

To conclude, we have presented upconverting nanoparticles that display an unprecedented upconversion quantum yield of ~ 7.5 % and strongly temperature-dependent upconversion characteristics under non-deoxygenated conditions. The nanoparticles were prepared by microemulsion of an emitter-terminated biocompatible and biodegradable poly(ε-caprolactone) in the presence of a metalloporphyrin sensitizer. Their thermoresponsive upconversion behavior permits insights into the fundamental mechanisms enabling the sTTA-UC process in the nanosized, isolated environment and the specific temperature is useful for in vivo temperature sensing. Heating the nanoparticles was shown to drastically reduce the lifetime of emitter triplets, usually in the milliseconds scale, which is responsible for the reduced upconversion quantum efficiency. As instruments with millisecond time resolution are widely available and inexpensive, this system is thus proposed as paradigm for a new class of time-gated fluorescent temperature nanosensors. We speculate that its design is general and that it can readily be adapted to other core materials and sTTA-UC chromophore pairs, allowing further developments that would improve the potential usefulness of the particles that were studied here as a first model system. While green to blue upconverting nanoparticles have been used for live-cell imaging and in-vivo monitoring in living mice,[26] better tissue penetration could be achieved with upconverting chromophore pairs absorbing in the near IR. Preliminary experiments further suggest that increasing the sensitizer content and/or its extinction coefficient may be beneficial or even necessary for single-particle imaging. Finally, the substitution of the adsorbed SDS with a covalently bound surfactant may be desirable, but in the light of previous studies this modification appears straightforward.[39]

Acknowledgements

The authors thank Dr. Sandor Balog and Dr. Stephen Schrettl for fruitful discussions and helpful comments. Funding from the Swiss National Science Foundation (grants number 200020_152968 and PP00P2133597/1) and the Adolphe Merkle Foundation is acknowledged. A. M. acknowledges support from the Università degli Studi Milano-Bicocca (grant n°2016-ATESP-0052).

Notes and references

1 C. A. Parker, in *Advances in Photochemistry*, John Wiley & Sons, Inc., Hoboken, NJ, USA, 1964, Volume 2, pp. 305–383.
2 C. A. Parker and C. G. Hatchard, *Proc. Chem. Soc.*, 1962, 386.
3 R. R. Islangulov, D. V. Kozlov and F. N. Castellano, *Chem. Commun.*, 2005, 3776–3778.
4 S. Baluschev, T. Miteva, V. Yakutkin, G. Nelles, A. Yasuda and G. Wegner, *Phys. Rev. Lett.*, 2006, **97**, 143903.
5 Y. Y. Cheng, T. Khoury, R. G. C. R. Clady, M. J. Y. Tayebjee, N. J. Ekins-Daukes, M. J. Crossley and T. W. Schmidt, *Phys. Chem. Chem. Phys.*, 2010, **12**, 66–71.
6 J. Zhao, S. Ji and H. Guo, *RSC Adv.*, 2011, **1**, 937–950.
7 A. Monguzzi, M. Frigoli, C. Larpent, R. Tubino and F. Meinardi, *Adv. Funct. Mater.*, 2012, **22**, 139–143.
8 Y. C. Simon, S. Bai, M. K. Sing, H. Dietsch, M. Achermann and C. Weder, *Macromol. Rapid Commun.*, 2012, **33**, 498–502.
9 J.-H. Kang and E. Reichmanis, *Angew. Chem. Int. Ed.*, 2012, **51**, 11841–11844.
10 C. Wohnhaas, A. Turshatov, V. Mailänder, S. Lorenz, S. Baluschev, T. Miteva and K. Landfester, *Macromol. Biosci.*, 2011, **11**, 772–778.
11 W. Wang, Q. Liu, C. Zhan, A. Barhoumi, T. Yang, R. G. Wylie, P. A. Armstrong and D. S. Kohane, *Nano Lett.*, 2015, **15**, 6332–6338.
12 C. Wohnhaas, V. Mailänder, M. Dröge, M. A. Filatov, D. Busko, Y. Avlasevich, S. Baluschev, T. Miteva, K. Landfester and A. Turshatov, *Macromol. Biosci.*, 2013, **13**, 1422–1430.
13 D. C. Thévenaz, S. H. Lee, F. Guignard, S. Balog, M. Lattuada, C. Weder and Y. C. Simon, *Macromol. Rapid Commun.*, 2016, **37**, 826–832.
14 Y. C. Simon and C. Weder, *J. Mater. Chem.*, 2012, **22**, 20817–21314.
15 C. E. McCusker and F. N. Castellano, *Top. Curr. Chem. (Z)*, 2016, **374**, 19–25.
16 A. Monguzzi, R. Tubino, S. Hoseinkhani, M. Campione and F. Meinardi, *Phys. Chem. Chem. Phys.*, 2012, **14**, 4322–4332.
17 S. H. Lee, M. A. Ayer, R. Vadrucci, C. Weder and Y. C. Simon, *Polym. Chem.*, 2014, **5**, 6898–6904.
18 S. H. Lee, D. C. Thévenaz, C. Weder and Y. C. Simon, *J. Polym. Sci. Part A: Polym. Chem.*, 2015, **53**, 1629–1639.
19 R. Vadrucci, C. Weder and Y. C. Simon, *J. Mater. Chem. C*, 2014, **2**, 2837.
20 X. Yu, X. Cao, X. Chen, N. Ayres and P. Zhang, *Chem. Commun.*, 2015, **51**, 588–591.
21 P. Mahato, A. Monguzzi, N. Yanai, T. Yamada and N. Kimizuka, *Nature Mater.*, 2015, **14**, 924–930.
22 T. Ogawa, N. Yanai, A. Monguzzi and N. Kimizuka, *Sci. Rep.*, 2015, **5**, 10882.
23 P. Mahato, N. Yanai, M. Sindoro, S. Granick and N. Kimizuka, *J. Am. Chem. Soc.*, 2016, **138**, 6541–6549.
24 N. Yanai and N. Kimizuka, *Chem. Commun.*, 2016, **52**, 5354–5370.
25 Q. Liu, B. Yin, T. Yang, Y. Yang, Z. Shen, P. Yao and F. Li, *J. Am. Chem. Soc.*, 2013, **135**, 5029–5037.
26 Q. Liu, T. Yang, W. Feng and F. Li, *J. Am. Chem. Soc.*, 2012, **134**, 5390–5397.
27 Q. Liu, W. Feng, T. Yang, T. Yi and F. Li, *Nature Protoc.*, 2013,

8, 2033–2044.
28 H.-Q. Peng, L.-Y. Niu, Y.-Z. Chen, L.-Z. Wu, C.-H. Tung and Q.-Z. Yang, *Chem. Rev.*, 2015, **115**, 7502–7542.
29 A. Turshatov, D. Busko, S. Baluschev, T. Miteva and K. Landfester, *New J. Phys.*, 2011, **13**, 083035.
30 A. Kumari, S. K. Yadav and S. C. Yadav, *Colloids Surf., B*, 2010, **75**, 1–18.
31 Y. P. Huang, X. Xu, X. L. Luo and D. Z. Ma, *Chi. J. Polym. Sci.*, 2002, **20**, 45–51.
32 S. U. Egelhaaf, E. Wehrli, M. Muller, M. Adrian and P. Schurtenberger, *J. Microsc.*, 1996, **184**, 214–228.
33 Y. Y. Cheng, B. Fückel, T. Khoury, R. G. C. R. Clady, M. J. Y. Tayebjee, N. J. Ekins-Daukes, M. J. Crossley and T. W. Schmidt, *J. Phys. Chem. Lett.*, 2010, **1**, 1795–1799.
34 M. Pope and C. E. Swenberg, *Electronic Processes in Organic Crystals and Polymers*, Oxford University Press, Second Edition. 1999.
35 A. Monguzzi, J. Mezyk, F. Scotognella, R. Tubino and F. Meinardi, *Phys. Rev. B*, 2008, **78**, 195112.
36 K. D. Wegner and N. Hildebrandt, *Chem. Soc. Rev.*, 2015, **44**, 4792–4834.
37 S. Lindén, M. K. Singh, K. D. Wegner, M. Regairaz, F. Dautry, F. Treussart and N. Hildebrandt, *Dalton Trans.*, 2015, **44**, 4994–5003.
38 K. Abe, L. Zhao, A. Periasamy, X. Intes and M. Barroso, *PLoS ONE*, 2013, **8**, e80269.
39 D. C. Thévenaz, C. A. Monnier, S. Balog and G. L. Fiore, *Biomacromolecules*, 2014, **15**, 3994–4001.

TOC Text and Figure

Low-power upconverting nanoparticles are presented that display highly efficient, temperature-dependent green to blue conversion under aerated aqueous conditions. These features are useful for live cell and in-vivo temperature sensing.